ON GRAVITY WAVES IN THE ATMOSPHERE

By Earl Gossard

Navy Electronics Laboratory [1]

and Walter Munk

University of California [2]

(Manuscript received 9 November 1953)

ABSTRACT

Seven times in a year's continuous observations, marked oscillations with periods from 5 to 15 minutes were simultaneously recorded on a barograph and a damped anemometer located at La Jolla, California. The oscillations often followed a reversal of the land- and sea-breeze regime, and they were sometimes preceded by a pressure pulse. Perturbations of pressure (p) and wind speed (v) attain double amplitudes up to several millibars and several meters per second, respectively, with maximum pressure occurring at the time of maximum "orbital" wind. This suggests propagating gravity waves in the atmosphere. Their velocity (C) can be inferred from the La Jolla records according to the impedance relationship, $p = \rho v C$; the computed arrival time at Point Loma, 11 miles to the south, agrees with the recorded arrival. Phase velocities are of the order of 10 m/s and greatly exceed ambient winds. Wavelengths range from 4 to 10 kilometers. A slight effect on sea level is apparent. Under steady meteorological conditions, there is good coherence for at least four wavelengths in the direction of propagation, but less coherence at right angles to this direction. The wave crests appear to be oriented normal to the wind shear between the upper and lower winds. The observed wave velocity is of the order given by the shallow "water" theory, *i.e.*, $(gh\,\Delta \ln \theta)^{\frac{1}{2}}$, where h is the elevation of the inversion layer, and $\Delta \ln \theta$ is the logarithmic change in potential temperature across this layer. The observed period is not inconsistent with the period $2\pi/s$ of the fundamental mode of the least dispersive (longest) "trapped" waves, where $s^2 = g\,d(\ln \theta)/dz$ is a measure of the stability *above* the inversion layer.

1. Introduction

Since 1950, continuous recordings of ocean waves with periods of 10 to 20 min have been made at the Scripps Institution of Oceanography in La Jolla. In early 1952, simultaneous recordings of atmospheric pressure and of appropriately damped wind-speed and -direction were added to the installation in the hope of finding some connection between the oceanic and atmospheric disturbances. It has developed that this *combination* of pressure records with suitably damped wind records offers a powerful method for investigating atmospheric gravity waves. The origin of the long ocean waves remains in doubt, but we seem to have learned something about waves some 2000 ft above the sea surface.

2. Instruments

Wind direction and speed.—A standard Friez *Aerovane* is located in a well exposed position at the end of Scripps' pier, about 30 ft above mean sea level and 1000 ft from shore. The aerovane actuates a linear servo unit, which drives a Selsyn. The Selsyn operates a linear potentiometer, which constitutes one-half of a balanced bridge. The propeller drives a d.c. generator. Both the bridge output and generator output are fed into integrating circuits with time constants compatible with the long-period ocean waves (see table 1).

Microbarograph.—The sensing unit is located in a flush pit at the shore end of the pier. It consists of a conventional aneroid cell, with the tension countering the vacuum provided by a suspended weight with a natural period of oscillation of something less than a second. The strain-gauge element is a balanced bridge whose output is recorded directly.

Barovariograph.—This is located at Point Loma, 11 mi south of Scripps (fig. 8), at an elevation of 350 ft above sea level. It is operated by the Exploratory Studies Section of the Navy Electronics Laboratory, to whom the writers are indebted for use of their records. The instrument is essentially a low-frequency microphone which has a "front" leak and a "back" leak into its two chambers. The response range is roughly from 12 sec to 6 min.

TABLE 1. Instrumental time constants, and resulting phase lags and amplitude reductions for waves of stated periods.

	Time const. (sec)	Phase lag (sec) 5 min	10 min	15 min	Amplitude factor 5 min	10 min	15 min
Wind direction	180	63	103	128	0.26	0.47	0.62
Wind speed	50	39	45	46	0.69	0.89	0.95

[1] Navy Electronics Laboratory Professional Contribution No. 27.

[2] Contribution from the Scripps Institution of Oceanography, New Series No. 720. This work has been supported by the Office of Naval Research.

The wind and pressure measurements at Scripps are recorded on a multi-channel Leeds and Northrup *Speedomax* together with air and sea temperature, and measurements of water level from the "tsunami recorders" (Munk *et al*, 1948) at Scripps and at Oceanside, 25 mi to the north-northwest of La Jolla. The recorder prints a dot for each of these measurements once every 38.7 sec (for example, fig. 1). This intermittent type of recording has been used to advantage in the analysis, for it provides a much more precise time scale than can be obtained under similar circumstances by a continuous record.

3. Observations

During the seven days listed in table 2, oscillations were recorded at the La Jolla installation. The observed data are summarized in lines 1–17. The observed periods (T) and frequencies ($\sigma = 2\pi/T$) are given in lines 7 and 8. Figs. 1–3 show the original records for the three best cases. Figs. 4 and 5 show the corresponding pilot-balloon and radiosonde data taken in San Diego, about 11 mi southeast of La Jolla. The definitions of the various velocity vectors are given in the legend to fig. 8.

Weather conditions.—In all cases, the oscillations occurred when there was a large temperature inversion over the area. The amount ($\Delta\theta$) and the elevations of the bottom (h) and top (h') of the temperature inversion are listed in lines 12–14 of table 2. This inversion was always quite low. In southern California such an inversion is often accompanied by fog or very low stratus (line 3). These conditions are usually found in the late summer or fall, when the southern California area is under the influence of a well-developed Pacific high-pressure system.

The ambient surface wind V (line 4) was very light, and the land- and sea-breeze sequence was usually well developed The oscillations often occurred after some directional change in the established surface flow.

The orbital winds.—From the original recordings of wind speed and direction, oscillating wind vectors were constructed, allowance having been made for the attenuations and phase lags introduced by the two instruments. The wind field was then resolved into a mean wind vector V and an orbital wind vector v (fig. 6). The construction was performed for each individual oscillation, or for two or three oscillations combined. Representative averages are given in line 4 for the mean winds, and in line 5 for the orbital winds. The ambiguity in orbital direction by 180 deg is discussed in the following section. It will be seen that in most cases the magnitude of the orbital wind

TABLE 2. Summary of observed and computed data for the seven occasions between April 1952 and May 1953 when marked oscillations occurred. Wave directions indicate directions *from* which waves are coming, in conformance with wind convention.

1. Date	4 April	27 July	4 Aug.	4 Sept.	2 Oct.	16 Oct.	16 Oct.	12 May
2. Time (PST)	1100 to 1300	0200 to 0310	1140 to 1400	0430 to 0530	0652 to 0710	0400 to 0600	0620 to 0720	0000 to 0040
3. Weather	Fog	Clear	Fog	Clear	Fog	Fog	Fog	Clear
				Tsunami recorder data				
4. V (m/s and dir.)	1.4/NNW	0.9/NE	2.9/W	2.2/N	1.2/WSW	0.8/NNE	0.9/NW	0.7/ENE
5. $2\,\Delta v$ (m/s and deg)	2.0/200	2.6/78	2.3/175	1.0/318	6.4/240	2.8/268	1.8/282	3.2/280
6. $2\,\Delta p$ (mb)	0.28	0.36	0.36	0.14	0.86	0.40	0.26	0.26
7. T (min)	14.0	7.5	6.5	5.5	8.5	7.5	7.5	11.0
8. σ (sec^{-1})	0.0075	0.014	0.016	0.019	0.012	0.014	0.014	0.0095
				San Diego pibal data				
9. Time (PST)	1300	0100	0700	0100	—	0100	0700	0700
10. V' (m/s and dir.)	1.4/SW	4.5/NNW	2.7/NW	7.6/NNW	—	1.8/W	5.0/ESE	3.6/N
				San Diego raob data				
11. Time (PST)	0700 and 1900	1900* and 0700	0700 and 1900	1900* and 0700	1900*	0700 and 1900	0700 and 1900	1900 and 0700
12. h (m)	170	170	300	260	210	180	180	100
13. h' (m)	600	670	1190	740	1000	670	670	400
14. $\Delta\theta$ (deg C)	15.0	14.0	20.0	10.5	11.5	17.5	17.5	6.0
15. s_1 (sec^{-1})	0.0086	0.0	0.0077	0.0	—	0.017	0.017	—
16. s_2 (sec^{-1})	0.037	0.030	0.028	0.031	0.024	0.035	0.035	0.025
17. s_3 (sec^{-1})	0.0086	0.010	0.0077	0.014	0.0056	0.0080	0.0080	0.0096
				Computed values				
18. C_i (m/s and deg)	12/200	12/78	13/175	12/318	11/240	12/268	12/282	6.7/280
19. $\bar{U}$ (m/s)	−0.6	+0.5	−0.6	+2.6	—	+0.07	+0.12	−0.09
20. L (km)	9.6	5.0	4.9	4.8	5.6	5.4	5.4	4.4
21. Two layers, L (km)	10.0	5.4	5.9	4.2	6.8	5.4	5.4	4.0
22. Three layers, L_I (km)	8.4	3.8	4.9	3.8	5.8	4.5	4.5	3.8
23. L_{II} (km)	2.8	1.2	1.7	1.2	1.9	1.5	1.5	1.3

* Preceding day.

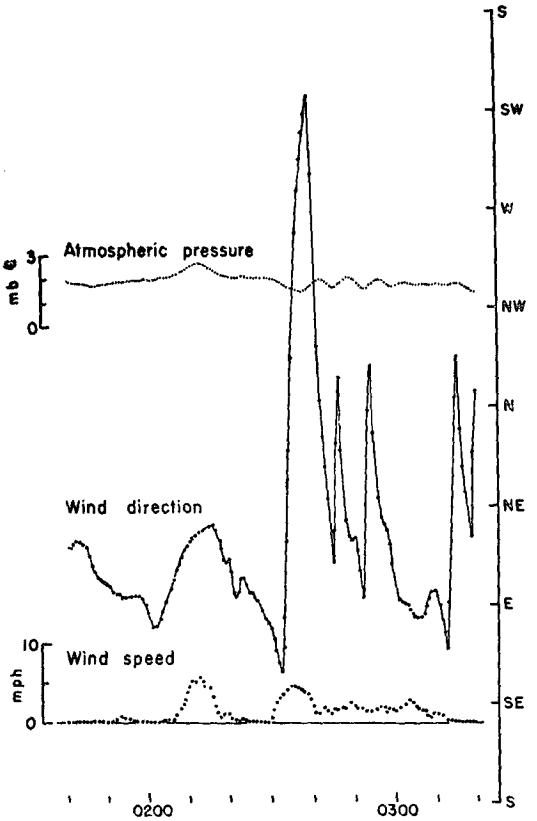

FIG. 1. *Speedomax* record for 27 July 1952. Scales for wind speed and direction apply to steady-state conditions; for short-period oscillations, allowance must be made for instrumental phase lag and attenuation (table 1).

actually exceeded that of the mean wind, so that the observed motion near the ground was largely the result (as will be shown) of internal wave activity. This corresponds to conditions found at the bottom of shallow stratified lakes.

An inspection of fig. 6 shows that the wind speed will reach maximum values for both directional extremes whenever the orbital motion is approximately at right angles to the mean wind vector, or when the mean wind vector is small. This accounts for the "double frequency" in the wind speed record (see fig. 3, 0400–0500 PST). If the orbital motion is approximately along the mean vector, the fundamental frequencies of wind speed and direction are the same. The relative frequencies and amplitudes of the two traces give, therefore, a quick indication of the orbital direction. It is clear that for simple harmonic motion both speed and direction records will depart in general from a sinusoidal form, and we have allowed for this as well as possible in correcting for instrumental characteristics. For very weak winds the instrumental threshold becomes an appreciable factor, and the measured values tend to be low and unreliable.

Phase relation between wind and pressure oscillations.—Fig. 7 shows the results of a cross-correlation between pressure and wind direction. The analysis was made for the exceptionally well defined oscillations occurring between 1223 and 1320 on 4 August (fig. 2). Values were read for successively printed points of pressure and direction, and the two traces were correlated. Thereupon the direction trace was displaced in time relative to the pressure trace by one point (38.7 sec) and a new correlation performed, *etc.* If the maxima in direction and pressure had occurred simultaneously, the maximum correlation should occur for the instrumental time lag of about 80 sec for 6½-min waves (table 1). Actually the optimum correlation occurs for about 93 sec. Thus, maximum pressure occurs at the time of maximum orbital wind. The orbital wind direction at the time of maximum pressure is given in line 5 of table 2.

Phase velocity and wave length.—The correlation between pressure and orbital motion strongly indicates that we are dealing with propagating waves (rather

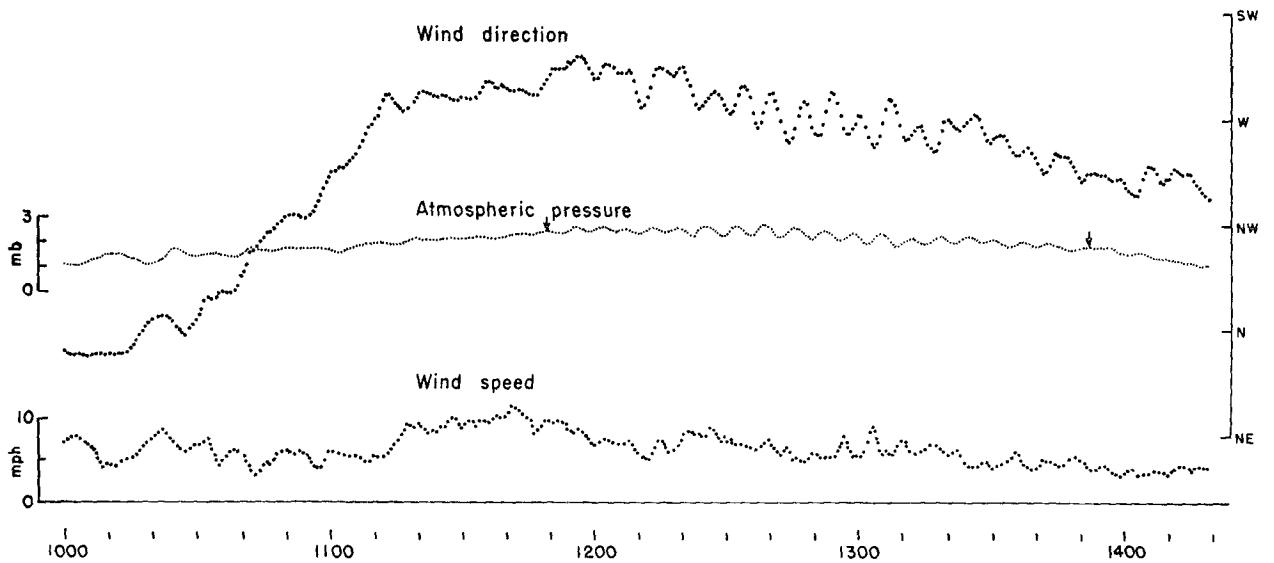

FIG. 2. *Speedomax* record for 4 August 1952. For comparison with Pt. Loma barovariograph (fig. 9), assumed duration of pressure disturbance is indicated by arrows.

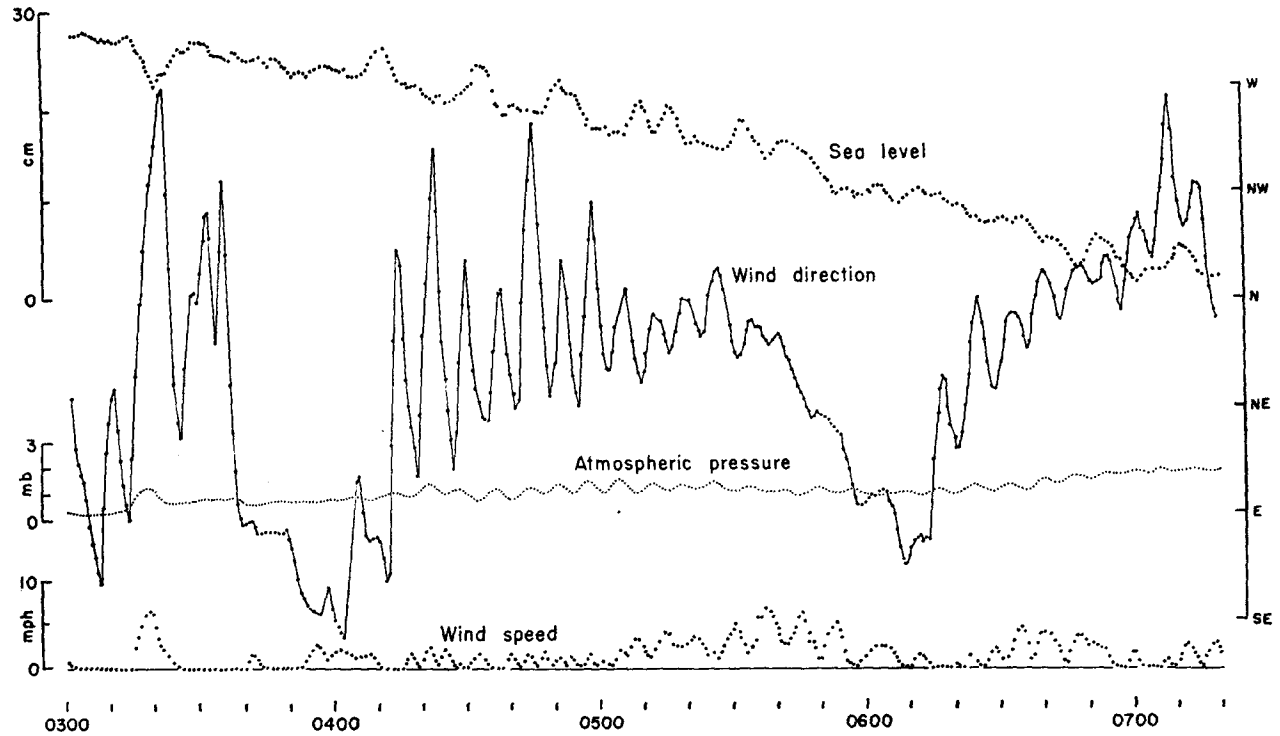

FIG. 3. *Speedomax* record for 16 October 1952. La Jolla sea-level record (cm) is included to show correlation with initial pressure pulse; remainder of record shows little correlation; sea level is recorded on La Jolla tsunami recorder. Scale appropriate to 9-min oscillations is shown on left; corresponding instrumental phase lag is 2 min.

than drifting convection cells, see section 4, below). If this is the case, a knowledge of both pressure and orbital motion permits us to compute phase velocity C_i. This velocity is in the plane of orbital motion; its direction is that of the orbital velocity v at the time of positive pressure perturbation[3] p, and its magnitude

[3] This is true not only for the theoretical models under consideration in section 5, below, but for gravity waves in general. In ocean waves, for example, maximum pressure and orbital motion in the direction of propagation both occur beneath the crest.

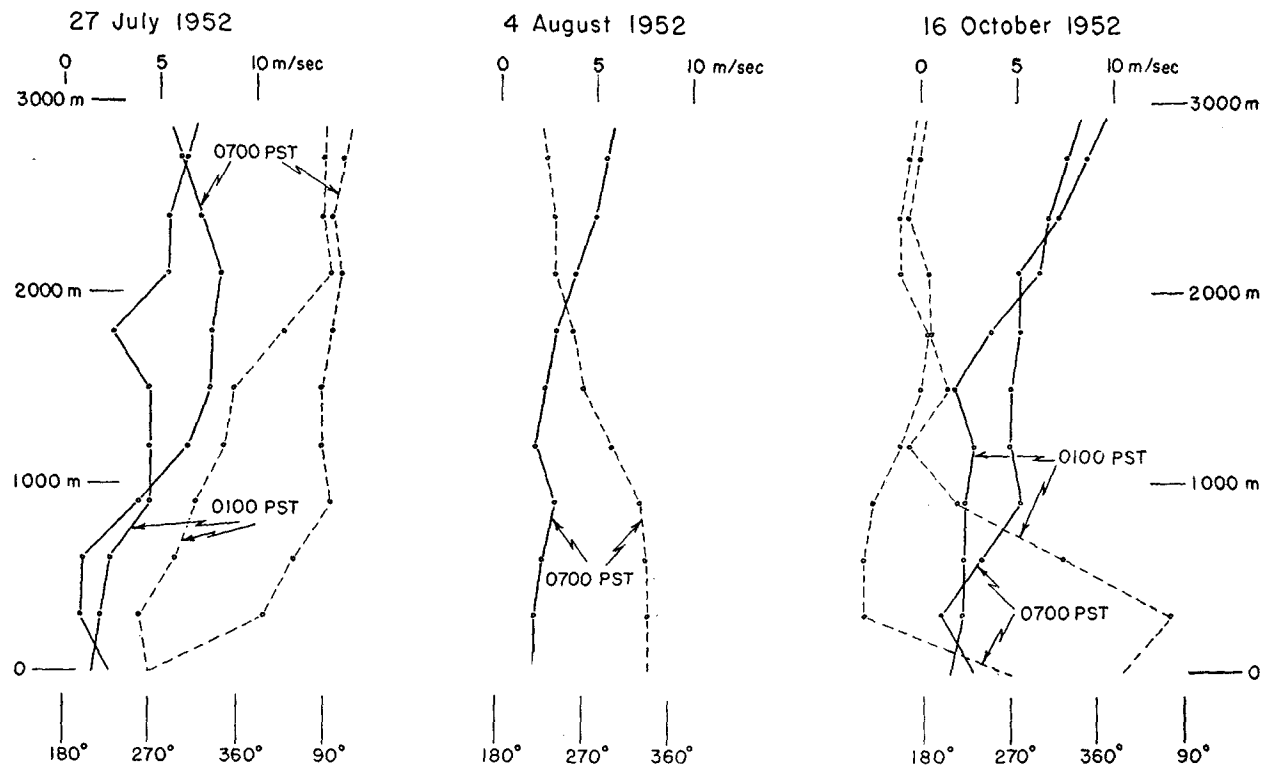

FIG. 4. Pilot-balloon observations for three days during which records in figs. 1–3 were taken. Solid lines connect measured values of wind speed. Dashed lines connect measured values of wind direction.

is given by the "impedance relationship," $C_i = p/\rho v$. Hence

$$\boldsymbol{C}_i = (p/\rho v)\, \boldsymbol{v}_1, \tag{1}$$

where $\boldsymbol{v}_1$ is a unit vector in the direction of $\boldsymbol{v}$ during positive p, and $v = \boldsymbol{v} \cdot \boldsymbol{v}_1$. This relationship is familiar in acoustics as a means of inferring orbital velocity from measured pressure and wave velocity.

Equation (1) follows from the horizontal equation of motion,

$$\rho\, \partial \boldsymbol{v}/\partial t + \rho \boldsymbol{V} \cdot \Delta \boldsymbol{v} = -\Delta p,$$

where $\boldsymbol{V}$ is the mean drift, and $\boldsymbol{v}$ is the perturbation velocity. For solutions of the type $\boldsymbol{v}, p \propto \exp i(\boldsymbol{m} \cdot \boldsymbol{r} - \sigma t)$, this gives

$$\rho \nu \boldsymbol{v} = p\boldsymbol{m}, \tag{2}$$

where

$$\nu = \sigma - \boldsymbol{m} \cdot \boldsymbol{V} \tag{3}$$

can be seen to be the frequency noted by an observer drifting with velocity $\boldsymbol{V}$, whereas σ is the frequency at a fixed point.[4] The perturbations are therefore transmitted in the direction of $\boldsymbol{v}_1$ with a speed $\nu/m = p/\rho v$ relative to the drifting observer. Hence $\boldsymbol{C}_i$ is the *relative* phase velocity. According to (1) and (2), $\boldsymbol{C}_i$ is in the direction of $\boldsymbol{m}$, hence perpendicular to the wave crests. In the presence of a mean wind, the travel time of a long crest between two points will be shortened or lengthened according to whether the wind blows in the direction of wave propagation or opposite, but the travel time will not be affected by a wind blowing along the crests. The absolute phase velocity $\boldsymbol{C}$ relative to the ground is therefore a vector in the direction of $\boldsymbol{C}_i$ (normal to the crests) with magnitude $C = C_i + U$, where U is the projection of $\boldsymbol{V}$ on $\boldsymbol{C}_i$. If the surface winds differ from the winds aloft, U must be replaced by an appropriately weighted average $\bar{U}$ [see (15)]; hence,

$$C = C_i + \bar{U}. \tag{4}$$

The travel time for a coherent crest between two recorders is then $\Delta x/C$, where Δx is the projection on $\boldsymbol{C}_i$ (and, of course, on $\boldsymbol{C}$) of the distance between the recorders. The wave length is $L = CT$, where T is the period recorded by fixed instruments.

Numerical values for $\boldsymbol{C}_i$, $\bar{U}$ and L are given in lines 18–20 of table 2. The values for wave speed and direction can be independently checked by comparison between computed and recorded arrivals at Point Loma (fig. 9). In most cases the waves travelled at nearly a right angle to a line connecting the recorders, and the calculation depends too critically on the measured orbital direction to provide a critical check on the velocity. However, on 4 August the wave direction was nearly parallel to the line between the recorders (fig. 8). The arrivals of the disturbance at the two stations (marked by arrows on figs. 2 and 9) correspond to a travel time of 23.5 min, compared to a computed value of 24.2 min. In this computation, phase velocity was used rather than group velocity, the two being nearly equal for the long waves here under consideration (see section 5, below).

[4] Strictly speaking, this applies only to one-directional propagation; but the results are only slightly modified if the "beam width" is narrow.

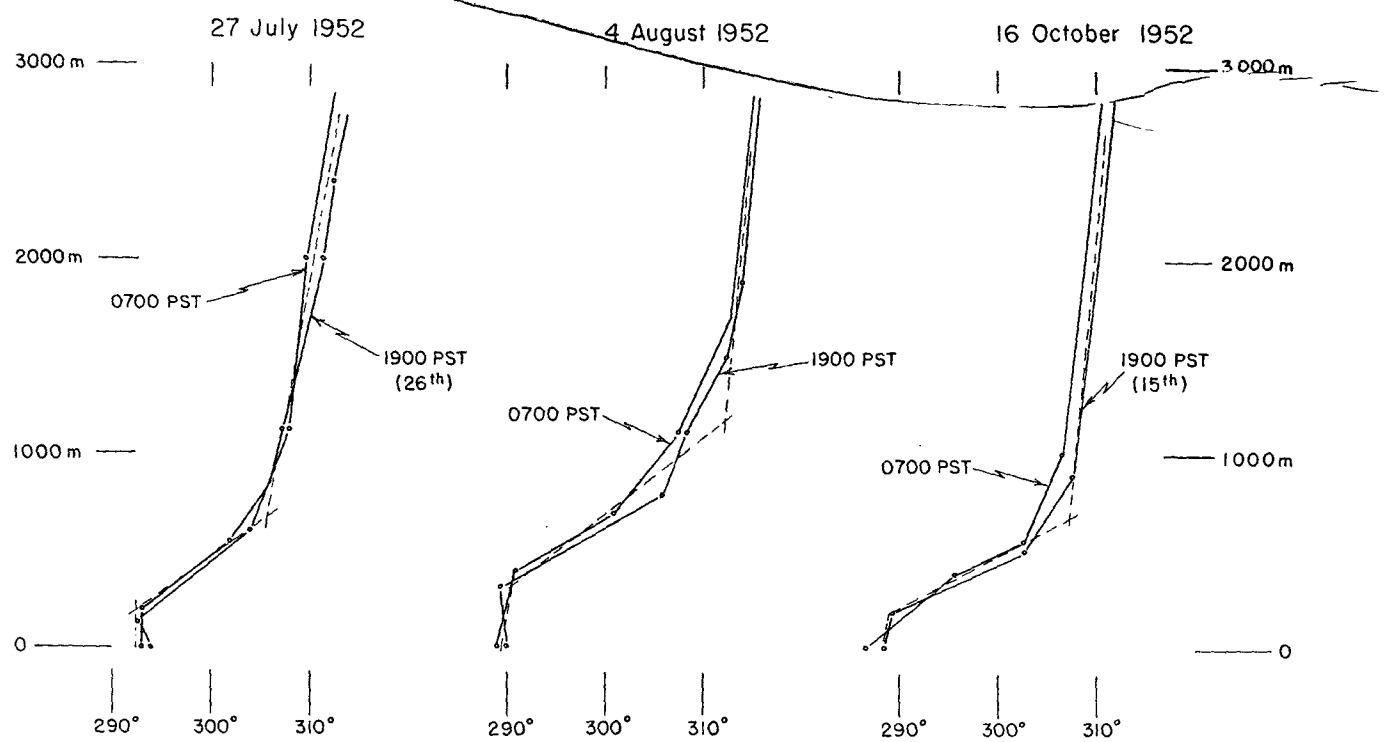

FIG. 5. Radiosonde observations for three days during which records in figs. 1–3 were taken. Solid lines connect observed values of potential temperature in deg K. Dashed lines indicate relationship assumed in theoretical models.

Coherence.—A comparison of the records in figs. 2 and 9 reveals good coherence at the two stations, which are separated by four wavelengths. Nineteen principal crests are identifiable. On days when the wave direction was more nearly normal to the line between the stations, the coherence was considerably poorer. The waves would therefore appear to be short-crested. It should also be noted that on 4 August the direction of propagation remained nearly uniform during the entire disturbance. On other occasions the direction of propagation changed rather rapidly, and the coherence along any fixed direction was not as good.*

Effect on sea level.—Correlation between pressure and sea-level oscillations is found at times. In fig. 3, the initial pressure pulse is clearly accompanied by a depression in sea level. The best correlation for the seven days under consideration is shown in fig. 11. In most cases, the correlation is not convincing. One factor might be that the tsunami recorder is peaked at a period of 45 min and is therefore relatively insensitive to the observed shorter periods.

* *Note added in proof.* On 15 May 1954, pronounced oscillations commenced at 0200 PST at San Diego and about an hour earlier at Los Angeles. Five stations in the San Diego area indicated propagation to be from WSW. If the disturbance is assumed to have been propagated with a group velocity appropriate to the observed frequency, the disturbance was placed roughly 575 mi out to sea. This was not inconsistent with the location of a secondary low center. The inversion over southern California was marked. The simultaneous occurrence of inversion conditions and a low this far south is unusual.

The situation was similar to the one on 2 October 1952. Upon re-examination, we find that a disturbance did arrive in Los Angeles about 4 hr after the arrival in San Diego. There may be a connection with a tropical storm off the coast of Mexico several days earlier.

In other cases, the cause of the disturbance appears to be local.

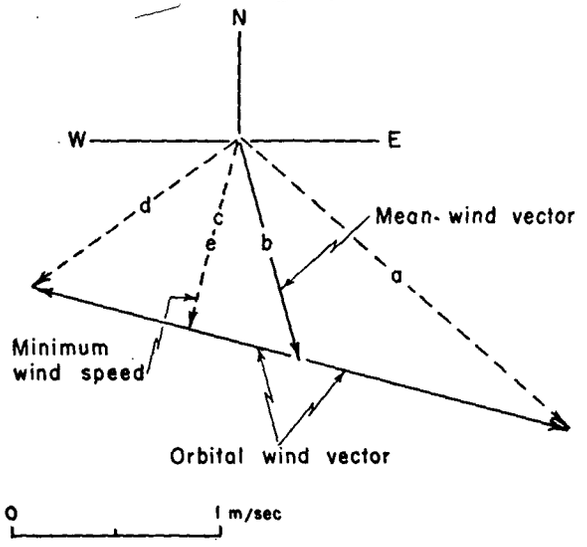

FIG. 6. Dashed arrows indicate wind vectors (pointing downwind) at five successive times, a, b, ... e, during interval 0501–0505 PST 16 October 1952. Construction is based on wind speed and direction records shown in fig. 3, allowing for instrumental characteristics. Oscillating wind vector has been resolved into mean vector, 1.1 m/s and 345 deg, and an orbital vector, 1.4 m/s and 285 and 105 deg.

4. Discussion

Waves or drifting convection cells.—The evidence favors waves. In the first place, the recorded travel time between La Jolla and Point Loma was of the order of 10 per cent of the time required for any disturbance drifting with the mean wind. Secondly, orbital velocity and pressure oscillations were in phase (see fig. 7) as they are in propagating waves, and not 90 deg out of phase as they are in convection cells. Thirdly, if we interpret the recorded fluctuations as being due to convection cells, their horizontal dimensions would be many times larger than their vertical dimension, taken as the elevation of the inversion base. This does not seem likely; convection theory indicates the proper ratio to be about 2:1. Finally, the occurrence of oscillations seems to be characteristic of great overall stability in the lower atmosphere.

It therefore seems reasonable to assume that the fluctuations were caused by some type of progressive waves. Phase velocities computed on the basis of this assumption [equation (1)] are in accordance with those observed.

Wave direction.—It was first stated by Wegener in 1908, and later supported by Trey's observations, that waves associated with billow clouds "are perpendicular to the wind shear" (Haurwitz, 1947). For the waves here under consideration, the average deviation from this law is 23 deg, compared to 45 deg for a random distribution in direction. In half the cases the waves travelled roughly in the direction $V' - V$, and in the other half in the direction $V - V'$. In this comparison it must be remembered that the upper wind observations were usually taken several hours before or after the oscillations occurred. Furthermore, by their very nature, pilot-balloon soundings smooth out and even erase abrupt discontinuities, making the choice of "upper" and "lower" winds quite arbitrary.

Somewhat more information can be gained by considering in detail the interval from 1100–1300,

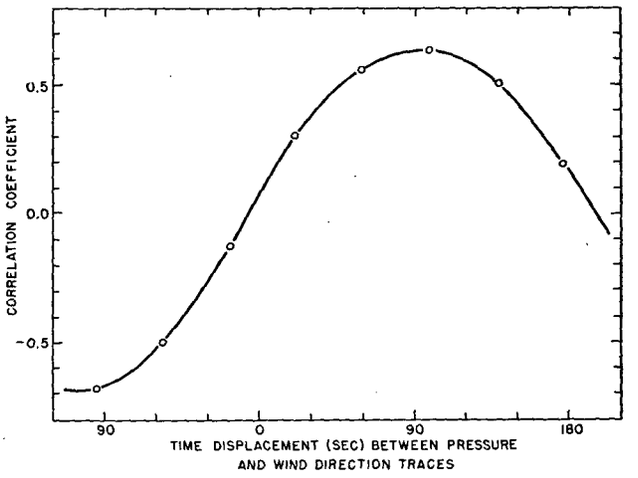

FIG. 7. Correlation between pressure and wind direction, 1223–1320 PST 4 August (fig. 2), for stated time displacements between two traces. Computed points are shown by circles.

4 August 1952, when the mean surface wind veered from WSW to WNW (fig. 10). The only available information concerning the upper wind is the 0700 pilot-balloon sounding at San Diego, giving 2.7 m/sec from NW (lines 9 and 10, table 2). However, it is known that reversal in the land- and sea-breeze sequence, or the onset of katabatic winds, often commences at the surface with winds at gradient level remaining at least temporarily unaffected. We therefore assume a steady upper-wind vector whose tip lies in the general area near P. As the surface wind veers, the shear vector must change accordingly, and by the above hypothesis the waves should travel along the line between the tip of the surface wind vector and P. It is seen that the observed wave direction does, in fact, vary roughly in the required fashion.

A similar analysis for the record of 16 October implies a weak upper wind from WNW at about 0500 PST, and a somewhat stronger wind from ENE

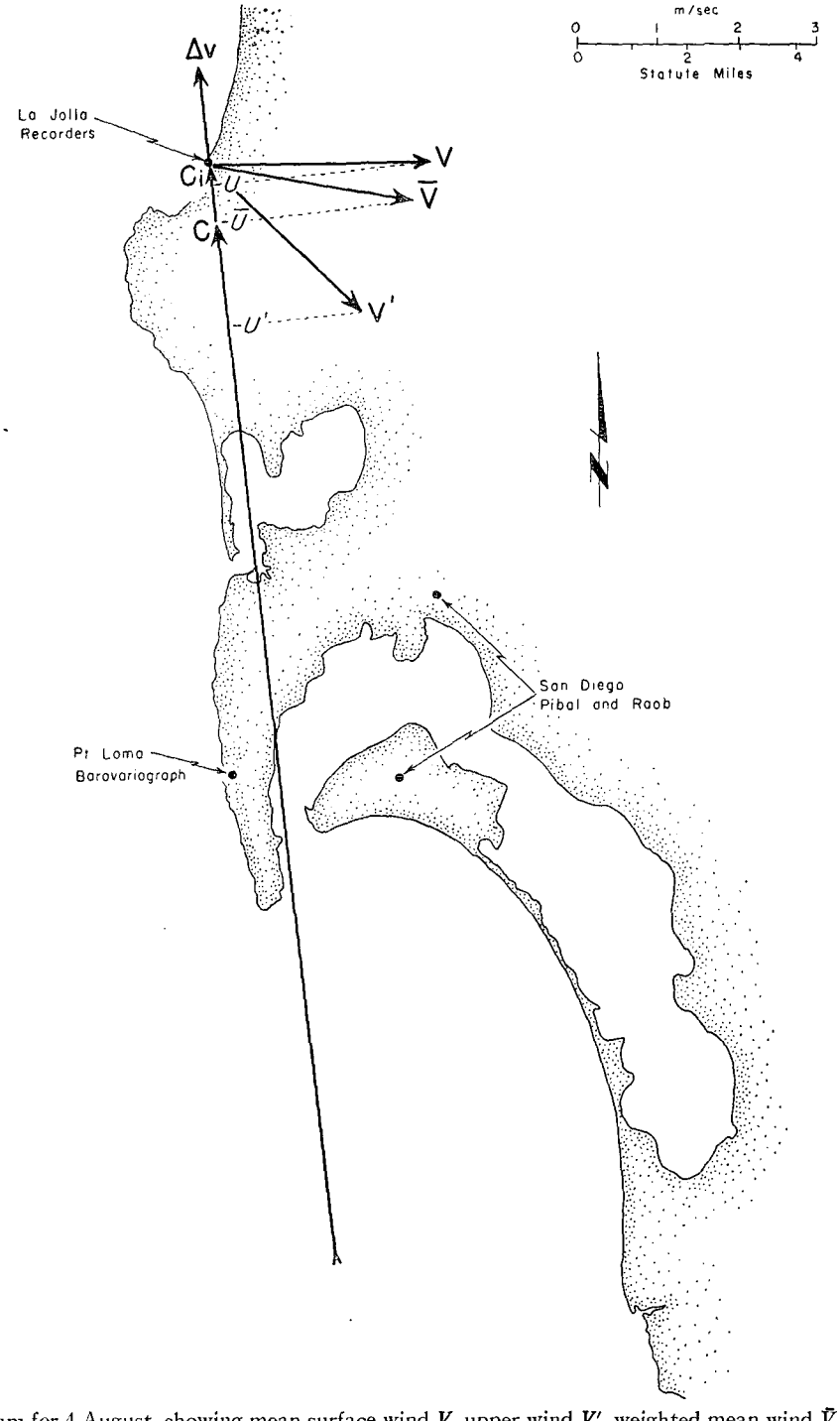

FIG. 8. Vector diagram for 4 August, showing mean surface wind V, upper wind V', weighted mean wind $\bar{V}$ [equation (15)], surface orbital wind Δv at time of maximum pressure, and "impedance wave velocity" C_i. Scalars U, U' and $\bar{U}$ refer to projections on $+C_i$ of surface, upper and mean winds. For case shown, these quantities are negative. Wave velocity C relative to ground is in direction of C_i and has magnitude $C_i + \bar{U}$. All arrows point downwind or "down wave." They are centered on underlying map on site of La Jolla recorders (V' is measured in San Diego). Location of the barovariogram at Point Loma is indicated.

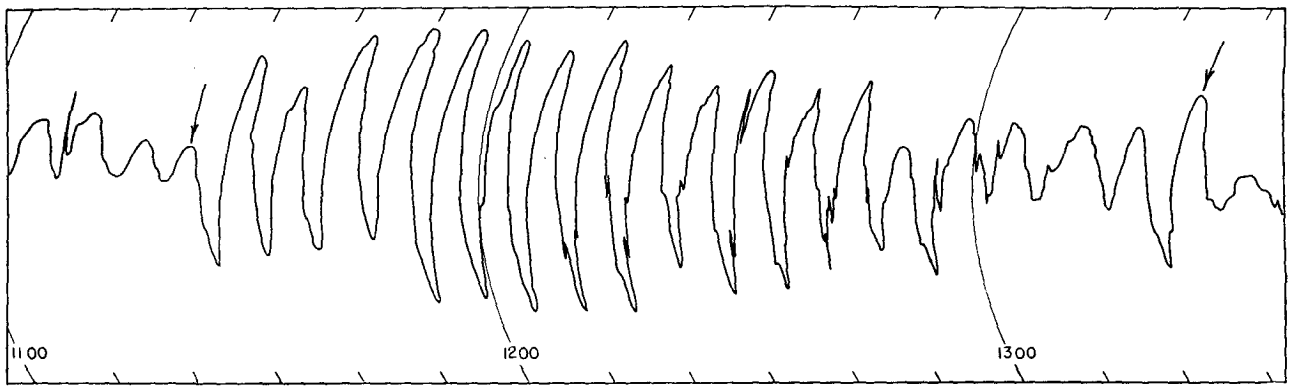

FIG. 9. Barovariograph record for 4 August 1952. For comparison with La Jolla record (fig. 2), assumed duration of disturbance is indicated by arrows. Full scale is approximately 0.5 mb.

after 0630. The San Diego pilot-balloon data show a strengthening and shift from W to ESE between 0100 and 0700 PST (lines 9 and 10, table 2).

On the basis of the above evidence, it can be said that the observations are not inconsistent with the assumption that the waves travel parallel to the wind shear. As seen from line 18, table 2, no particular direction is dominant, and the orientation of the coastline seems immaterial.

Wave velocity.—In the theory of billow clouds, it is often assumed that wave and wind speed are of the same order. Here we find $C \approx 10\ \bar{U}$ (lines 18 and 19, table 2).

5. Comparison with theory

Even a largely descriptive account, such as this one, would be incomplete without some comparison with theory. The theory of internal waves is well developed, due largely to the efforts of Helmholtz, Hoiland, Fjeldstad and Taylor. However, none of the published solutions is quite applicable to the present case. By following the general scheme in the developments by Fjeldstad (1933) and Queney (1946), we can give an abbreviated account.

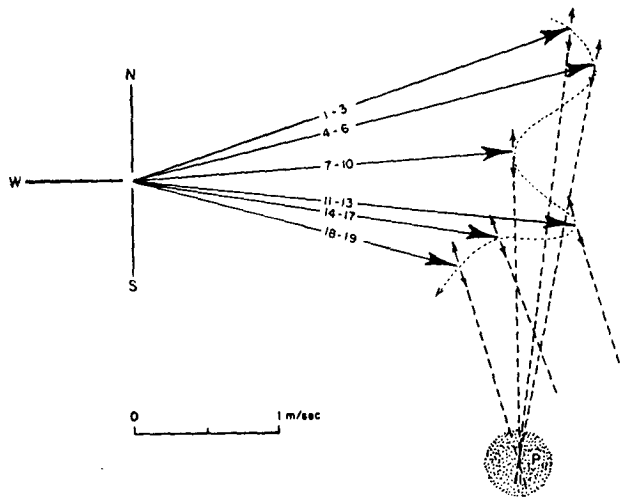

FIG. 10. Arrows drawn from origin point downwind in direction of mean surface wind during interval 1100–1300 PST 4 August 1952. Two-pointed arrows at end of wind vectors give orientation, but not strength, of orbital winds. Construction follows method shown in fig. 6. Dashed lines are extensions of orbital vectors in direction of wave propagation. Waves occurring during interval were numbered 1, 2, ... 20, and three or four successive waves combined into averages, as designated. Most of dashed lines converge in vicinity of P.

Perturbation equations.—The perturbation equations of motion, continuity and of the first law of thermodynamics for isentropic change are

$$\dot{v} + (1/\rho_0)\,\nabla p = -(\rho/\rho_0)g, \qquad (3, 4, 5)$$

$$(1/\rho_0)(\dot{\rho} + w\,d\rho_0/dz) = -\nabla\cdot v, \qquad (6)$$

and

$$\dot{\rho} + w(d\rho_0/dz) = c^{-2}(\dot{p} - \rho_0 g w), \qquad (7)$$

where $p_0(z)$ and $\rho_0(z)$ are the unperturbed distributions of pressure and density, c is sound velocity, and $(\cdot)$ designates the substantial derivative following the unperturbed flow (assumed not to vary continuously). The remaining notation is conventional. Eliminating ρ and using the relationship $s^2/g = 2S - g/c^2$, where

$$s^2 = g\,d(\ln\theta)/dz \text{ and } S = -\tfrac{1}{2}\,d(\ln\rho_0)/dz, \qquad (8)$$

we obtain

$$\ddot{w} = -\frac{1}{\rho_0}\left(\frac{\partial}{\partial z} + \frac{g}{c^2}\right)p - s^2 w, \qquad (5a)$$

and

$$\nabla\cdot v = -(1/\rho_0 c^2)\dot{p} + (g/c^2)w. \qquad (6a)$$

Equations (3), (4), (5a) and (6a) are linear and homogeneous in the four dependent variables $\rho_0^{\frac{1}{2}}v$ and $\rho_0^{-\frac{1}{2}}p$ (Queney, 1946). Furthermore, this system of equations has constant coefficients, provided s, S and U are constants over specified height intervals.[5] Here U designates the component of the (unperturbed) drift in the direction of wave propagation. Without loss in generality, we can take the x-axis in this direction and assume solutions of the form $\exp i\,(mx \pm nz - \sigma t)$. This leads to the dispersion equation,

$$\nu n^2 = m^2(s^2 - \nu^2) - \nu^2 S^2 + \nu^4 c^{-2}. \qquad (9)$$

[5] The case of a continuous shear has been examined by Sekera (1948); but since we observe $U \ll C$ in all cases, this extension is not critical here.

For the observed frequencies and wavelengths, this reduces to

$$\nu^2 n^2 = m^2(s^2 - \nu^2). \tag{9a}$$

Here

$$\nu = \sigma - Um \tag{10}$$

is the frequency noted by an observer drifting with the wind.

Boundary conditions.—Fig. 5 shows that the measured profiles of potential temperature can be represented by:

1. a lower mixed layer, from $z = 0$ to $z = h$;
2. a stable (inversion) layer, from $z = h$ to $z = h'$;
3. a layer with two-thirds to three-fourths the dry-adiabatic lapse rate, above $z = h'$.

Mean values of h, h', s_1, s_2 and s_3 are given in table 2.

We shall derive solutions for two special cases: (a) a simplified two-layer model with a wind and density discontinuity at the boundary $h'' = \frac{1}{2}(h + h')$ midway in the inversion layer, and with s_1, U, and s_3, U' referring to the lower and upper layers, and (b) a continuous three-layer model with no shear in the mean wind field. In the two-layer model, U and U' refer again to the projection of the wind vectors along the direction of propagation. The crosswind components are not excluded in the derivation, but their existence does not affect the solution. In the three-layer model, we have assumed

$$\nu_1 = \nu_2 = \nu_3 = \bar{\nu} = \sigma - \bar{U}m, \tag{11}$$

where $\bar{U}$ is the projection of a weighted mean wind (line 19, table 2) in the direction of wave propagation.

Equations (9) and (10) hold in each of the layers, but in the general case S_k, s_k, ν_k, U_k and n_k ($k = 1, 2, 3$) are different in each of the layers, whereas m and σ are the same throughout. The solutions for the different layers are patched together by requiring w and

$$d(p_0 + p)/dt = \dot{p} + w\, dp_0/dz \tag{12}$$

to be continuous across the interfaces.[6] With the additional boundary conditions

$$w_1 = 0 \text{ at } z = 0 \text{ and } w_3 \neq \infty \text{ at } z = \infty, \tag{13}$$

and the relationship (5a) between w and p, we can evaluate the six constants c_k and d_k in

$$w_k = e^{S_k z}(c_k e^{in_k z} + d_k e^{-in_k z})\, e^{i(mx - \sigma t)}.$$

Solutions.—The derivation of the solutions is cumbersome and uninteresting. For the two-layer model, the result is a slightly generalized Helmholtz equation,

$$\frac{\bar{\nu}}{m} = \frac{\sigma}{m} - \bar{U}$$

$$= \pm\left[\frac{g\,\Delta\theta}{A_1 + A_3} - \frac{A_1 A_3}{(A_1 + A_3)^2}(U' - U)^2\right]^{\frac{1}{2}}, \tag{14}$$

where

$$\bar{U} = (A_1 U + A_3 U')/(A_1 + A_3) \tag{15}$$

is a weighted average wind, $\Delta\theta = (\theta_3)_{z=h''} - (\theta_1)_{z=h''}$

[6] For the three-layer model, $\rho_0(z)$, and hence $w\, dp_0/dz$, is already continuous across the interfaces.

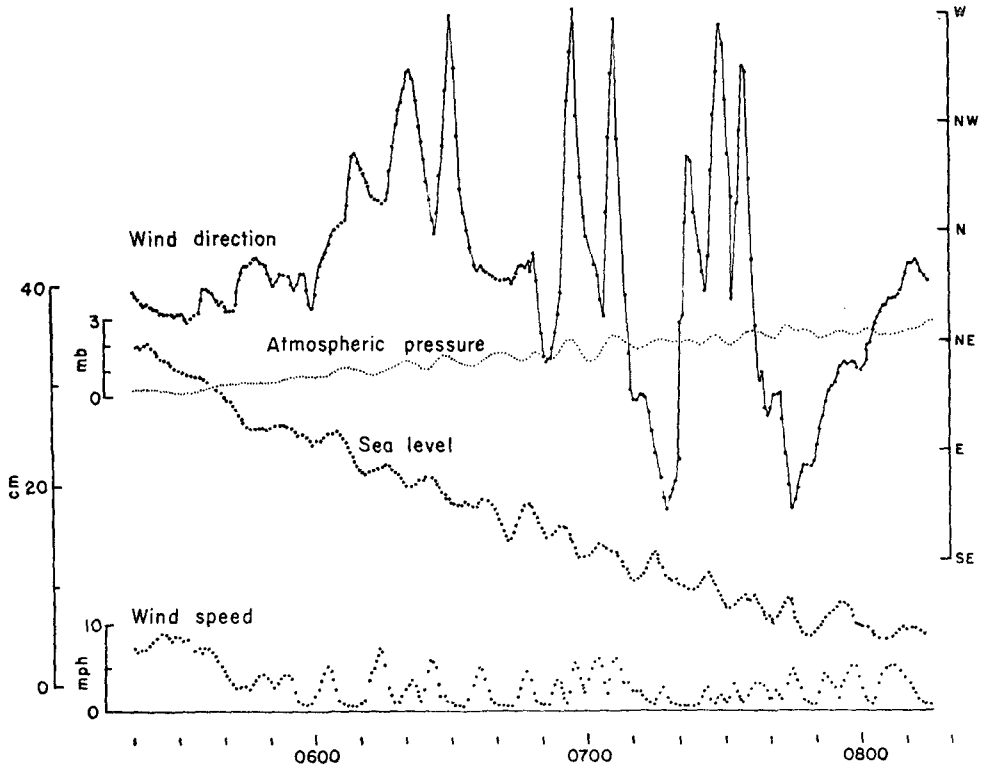

FIG. 11. *Speedomax* record for 2 October 1952, including sea level (cm) as recorded on La Jolla tsunami recorder. Sea-level scale is appropriate to oscillations of 9-min period. Corresponding instrumental phase lag is 2 min.

is the discontinuous change in potential temperature across the boundary, $A_1 = (\theta_1)_{z=h''}\ \gamma_1 \coth(\gamma_1 h'')$, and $A_3 = (\theta_3)_{z=h''}\ \gamma_3$, with γ_1 and γ_3 denoting $-in_1$ and $-in_3$. For the three-layer case,

$$n_2 \cot n_2(h'-h) = \frac{(S_3-S_2-\gamma_3)(S_1-S_2+\gamma_1 \coth \gamma_1 h)+n_2^2}{S_1-S_3+\gamma_3+\gamma_1 \coth \gamma_1 h}. \quad (16)$$

The terms S_1, S_2 and S_3 can be neglected, provided the unperturbed density changes a small fraction of its mean value in the part of the atmosphere affected by wave motion. Across a thin inversion layer, $\Delta(\ln\theta)$ and $n_2(h'-h)$ are small numbers. The above equation then yields a fundamental mode,

$$C^2 = (g\,\Delta\theta)/(A_1 + A_3), \quad (16a)$$

in agreement with the two-layer formula (14) for $U = U' = \bar{U}$. The simplest case is that of a shallow layer, $\gamma_1 h \ll 1$, and $\gamma_1 \approx \gamma_3$, as observed. Then,

$$C^2 = gh\,\Delta(\ln\theta). \quad (16b)$$

The two solutions (14) and (16) are plotted in fig. 12, with the here unimportant wind terms omitted. For the case under consideration, we may also neglect the S's and set $s_1 = s_3$. Consider any point on the curves $\sigma(m)$. The slope of the line from the origin through this point is the phase velocity σ/m, and the tangent $d\sigma/dm$ is the group velocity.

For all frequencies between (s_1, s_3) and s_2, the vertical wave numbers n_1 and n_3 are imaginary, and n_2 is real [equation (9a)]. Hence the assumed solutions $\exp i(mx \pm nz - \sigma t)$ are vertically trigonometric, or *cellular*, in the inversion layer, and hyperbolic in the lower and upper layers (fig. 13). This means that wave motion essentially vanishes a distance $1/\gamma_3$ above the inversion layer, *i.e.*, that the wave energy is *trapped* in the lower atmosphere.

There are no solutions for frequencies larger than s_2, other than sound waves. The two-layer case may be considered a special case of the three-layer model in which the middle (inversion) layer has collapsed, so that $s_2 \to \infty$, and σ is unbounded for large m.

For frequencies less than s_3, the upper wave number n_3 is real, and the cellular solution extends to infinite height. Both solutions yield complex frequencies, and hence the wave amplitudes must vary with time. The physical interpretation is that these *untrapped* modes radiate energy into the upper atmosphere. In analogy with the "potential trap" problem in quantum mechanics (*e.g.*, Rasetti, 1936, pp. 100–114; Condon and Morse, 1929, pp. 228–231), we may expect continuous spectra (noise) for this range of frequencies in addition to the discrete spectral lines $\sigma_I(m)$, $\sigma_{II}(m)$, . . . *etc.* Here it may turn out that solutions are essentially modified if s is not constant above a certain height, as here assumed, but only approaches a constant asymptotically.

A proper treatment of these problems that arise when $\sigma \ll s_3$ involves the solution to the appropriate initial value problem. We have not attempted this here. In all events, for waves generated at some distance by a disturbance in the lower layers, those most likely to persist at the lower levels are the trapped modes. These include the fundamental and various overtones (such as curves I and II in figs. 12 and 13), and for each of these modes all frequencies between s_3 and s_2 are possible. Which of these modes and frequencies will be the most prominent depends on three considerations: (1) how these oscillations are initially excited, (2) how they are transmitted, and (3) how they are recorded.

If the initial disturbance is so large that its spectrum contains only wave numbers smaller than m_I (wavelength larger than $2\pi/m_I$), no trapped modes at all will be excited (fig. 12). If the disturbance spectrum

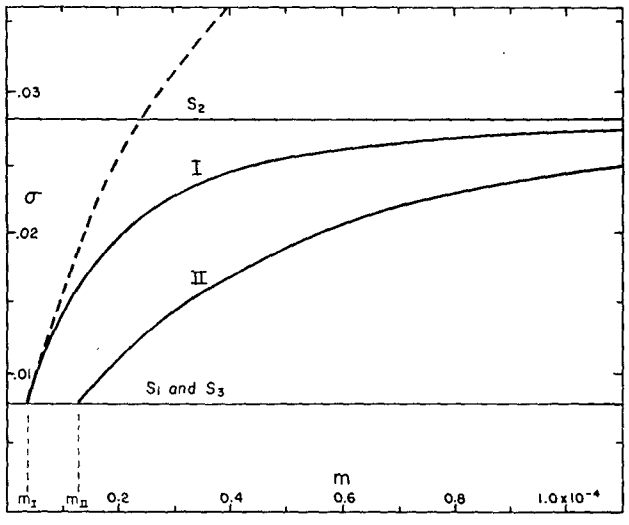

FIG. 12. Plot of frequency σ (sec^{-1}) as function of wave number m (cm^{-1}), pertaining to conditions on 4 August. For frequencies less than s_1 or s_3, σ is complex. Solid lines refer to fundamental (I) and second mode (II) of three-layer model (16). Dashed line refers to two-layer model (14).

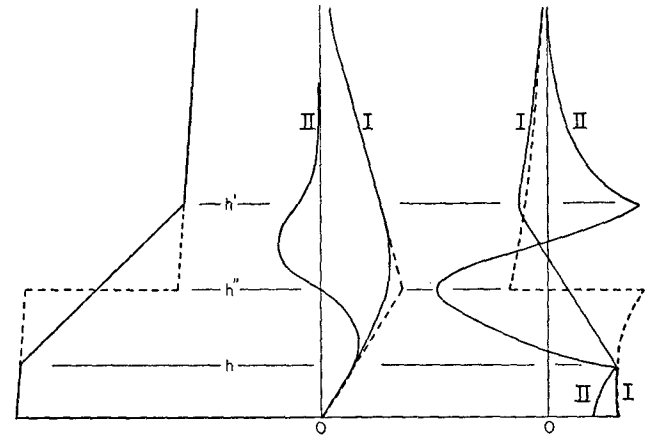

FIG. 13. Left: assumed distribution of potential temperature for two-layer (dashed) and three-layer (solid) models. Middle: corresponding distributions of vertical velocity, including two gravest modes for three-layer case. Right: corresponding distributions of pressure or horizontal velocity.

extends just past m_I, waves of wave number m_I and frequency $\sigma(m_I) = s_3$ of the fundamental mode are excited. If it extends up to, but not including, m_{II}, the oscillation is still limited to the fundamental mode, but it now consists of a "wave packet" containing all wave numbers between m_I and m_{II} and the corresponding frequencies $\sigma(m_I)$ to $\sigma(m_{II})$ along the line marked I. If the disturbance spectrum extends past m_{II}, waves of the second mode are also excited, *etc.* Hence, large disturbances will tend to generate waves of the fundamental mode and of frequencies near s_3.

Once a wave packet is formed, it will spread in horizontal extent, because the shorter waves move slower than the longer waves. The most prominent will be the least dispersive components, other factors remaining equal. The least dispersive waves will be those nearest the origin in fig. 12, for which the group velocity is most nearly constant and equal to the phase velocity.

Finally, higher modes will have proportionally lower amplitudes near the ground (where they were recorded). For very high modes, $\gamma_1 h \gg 1$, and the pressure disturbance hardly reaches the ground at all. In the case of a thin inversion layer, all modes higher than the fundamental die off rapidly above and beneath, and in the extreme two-layer case they vanish altogether at both sides of the infinitely thin inversion layer. This accounts for the absence of all higher modes in the two-layer model. Under the observed conditions (fig. 13), the second mode is only one-third lower at the ground than the fundamental mode, other factors remaining equal. This alone cannot account for the apparent absence of higher modes in the records.

Comparison between theoretical and observed wavelengths.—For the observed values of $\bar{U}$, the "Doppler shift" is small; hence, σ and $\bar{\nu}$ are nearly equal. It will be noted that $s_1 < \bar{\nu}$, $s_2 > \bar{\nu}$ and $s_3 < \bar{\nu}$. According to (8), n_1 and n_3 are then imaginary, n_2 is real, and (14) and (16) contain only real quantities. The equations have been solved for the horizontal wavelength $2\pi/m$, *with use of the observed values of* σ and ambient winds (lines 4, 8 and 10, table 2). Only the two gravest modes of an infinite number of roots to (16) have been evaluated.

The resulting wavelengths (lines 21 to 23, table 2) are of the same order of magnitude as those in line 20, which were derived from the impedance relation (1) and may be regarded as observed values. If $n_2 \Delta h \ll 1$, the two- and three-layer models should both yield values according to (16a). The two models do, in fact, yield similar values because $n_2 \Delta h < 1$ (but not $\ll 1$). The values are of the same order as those obtained by using the shallow "water" approximation (16b). The agreement is better for the fundamental mode L_I than for L_{II}, indicating a disturbance whose dimensions exceed L_I ($\approx$ 10 km).

Comparison between theoretical and observed wave periods.—In the theoretical discussion, it has been shown that waves of the fundamental modes and of low frequency are the ones most likely to be excited by a large initial disturbance (if there was one), that the least dispersive (longest) trapped waves are the ones most likely to persist and to be prominent near the ground (where the recordings were made). Hence, we should expect[7] frequencies between s_3 and s_2 and closer to s_3. This is roughly what the observations show (lines 8, 16 and 17, table 2).

The evaluation of s_3 is a matter of some uncertainty. The transition from the inversion layer to the upper air layer is not in reality abrupt, as assumed, and the selection of the effective upper lapse rate must remain to some extent arbitrary (see fig. 5). Furthermore, the soundings were not taken at the time and place of the recorded oscillations. With these shortcomings in mind, the observed frequencies are not inconsistent with foregoing conclusions, even though the agreement is not always impressive.

Acknowledgments.—Profs. Jörgen Holmboe and Carl Eckart of the University of California, and Miss Elisabeth Flauraud of the Air Force Cambridge Research Center, have made many helpful suggestions. The writers also wish to express their appreciation to Dr. J. B. Smyth of the Navy Electronics Laboratory, whose generous cooperation made the present joint effort possible. Mr. Charles Johnson of the Navy Electronics Laboratory has made the barovariograph record available to us. Mr. James Snodgrass, with the assistance of Heber Blair, has been largely responsible for the La Jolla installation.

REFERENCES

Condon, E. U., and P. M. Morse, 1929: *Quantum mechanics.* New York, McGraw-Hill, pp. 228–231.

Fjeldstad, J. E., 1933: Interne Wellen. *Geofys. Publ.*, **10**, No. 6, 35 pp.

Haurwitz, B., 1947: Internal waves in the atmosphere and convection patterns. *Ann. N. Y. Acad. Sci.*, **48**, 727–744.

Martyn, D. F., 1950: Cellular atmospheric waves. *Proc. roy. Soc. London*, **201**, 216–234.

Munk, W. H., H. V. Iglesias, and T. R. Folsom, 1948: An instrument for recording ultra low frequency ocean waves. *Rev. Sci. Instrum.*, **19**, 654–658.

Queney, P., 1947: Theory of perturbations in stratified currents with application to air flow over mountain barriers. *Univ. Chicago, Dept. Meteor., Misc. Rep.*, No. 23, 80 pp.

Rasetti, F., 1936: *Elements of nuclear physics.* New York, Prentice-Hall, pp. 100–114.

Sekera, Z., 1948: Helmholtz waves in a linear temperature field with vertical wind shear. *J. Meteor.*, **5**, 93–102.

[7] This is the conclusion reached by Martyn (1950) in a study of a two-layer model consisting of an upper layer and a ground-based inversion layer. Martyn assumes linear (rather than exponential) gradients in potential temperature. This complicates the solutions greatly without affecting numerical values appreciably. He also replaces the condition, $\partial p/\partial t$ continuous across the layers, by the boundary condition of a free surface at the inversion, $\partial p/\partial t = 0$. For a shallow inversion layer, this leads to the relationship $C\pi(s_2^2 - \sigma^2)^{-\frac{1}{2}}(\Delta h)^{-1} = 1/j$ instead of $= 2/(2j - 1)$, where $j = 1, 2, \cdots$ refers to the fundamental and higher modes. Thus, we obtain phase velocities about twice those of Martyn and in closer agreement with our observations.